JOURNAL OF GUIDANCE, CONTROL, AND DYNAMICS
Vol. 28, No. 5, September–October 2005

Analytical Control Laws for Planet-Centered Solar Sailing

Malcolm Macdonald*
University of Glasgow, Glasgow, Scotland G12 8QQ, United Kingdom
and
Colin R. McInnes†
University of Strathclyde, Glasgow, Scotland G1 1XJ, United Kingdom

With increased interest in solar sailing from both ESA and NASA for future science missions comes the requirement to assess potential planet-centered orbits and generate algorithms for effective orbit maneuvering and control. Previous planet-centered solar-sail trajectory work has been limited mostly to Earth-escape or lunar flyby trajectories as a result of the difficulties of fully optimizing multirevolution orbits. A new method of blending locally optimal control laws is introduced, where each control law is prioritized by consideration of how efficiently it will use the solar sail and how far each orbital element is from its target value. The blended, locally optimal sail thrust vector is thus defined to use the sail as efficiently as possible, allowing the rapid generation of near-optimal trajectories. The blending method introduced is demonstrated for a complex orbit transfer and for two stationkeeping applications. Furthermore, the algorithms developed are explicitly independent of time, and as such the control system is demonstrated suitable as a potential future onboard sail controller.

Nomenclature

a	=	semimajor axis
$\boldsymbol{a}_s$	=	sail acceleration
a_{s_c}	=	sail characteristic acceleration
E	=	eccentric anomaly
e	=	eccentricity
F	=	disturbing acceleration within variational equations of motion
f	=	modified equinoctial element
$\boldsymbol{f}_k$	=	sail normal vector for element k
$\boldsymbol{f}_s$	=	orbit perturbation vector caused by sail, $= [F_R \;\; F_T \;\; F_N]$
g	=	modified equinoctial element
h	=	modified equinoctial element
i	=	orbit inclination
k	=	modified equinoctial element
L	=	modified equinoctial element
p	=	semilatus rectum
r	=	orbit radius
$\boldsymbol{r}$	=	radius vector
r_p	=	radius of pericenter
t	=	time
W	=	weight of control law
α	=	sail pitch angle
$\tilde{\alpha}$	=	pitch angle of ideal force vector
δ	=	sail clock angle
$\boldsymbol{\lambda}_b$	=	blended locally optimal force vector $[x_b \;\; y_b \;\; z_b]^T$
$\boldsymbol{\lambda}_k$	=	function of orbit elements, $= [\lambda_x \;\; \lambda_y \;\; \lambda_z]^T$ for element k
μ	=	gravitational parameter
ν	=	true anomaly
ς	=	spacecraft shadow parameter
ς_p	=	penumbra critical shadow parameter
τ	=	auxiliary positive variable
Ω	=	right ascension angle of ascending node
ω	=	argument of pericenter

Subscripts

M	=	Mercury
sat	=	spacecraft
sun → M	=	sun with respect to Mercury
sun → sat	=	sun with respect to spacecraft

Introduction

SOLAR sailing is increasingly being considered by both ESA and NASA for future science missions. From the absence of reaction mass from the primary propulsion system arises the potential for new high-energy mission concepts, such as a Solar Polar orbiter, an Interstellar Heliopause Probe, and planetary sample return missions.[1,2] Planet-centered solar-sail trajectory analysis has been limited in range, such as simple Earth-escape strategies that provide crude estimates of escape time and often physically impossible orbits caused by negative altitude passes at perigee.[3–6] Other planet-centered applications that have been studied in detail include lunar flyby[7,8] or potential simple orbit maneuvering capabilities.[9]

In the late 1970s Sackett produced optimal solar-sail transfers and Earth-escape trajectories, which, although they did not include orbit perturbations, they did note a tendency for optimal and near-optimal solar-sail orbits to require very low, often negative, altitude passes of Earth.[10,11] This problem was suitably addressed by inclusion of a penalty function. Subsequent work has failed to redress this problem, neglecting and dismissing the inclusion of minimum altitudes on Earth-escape trajectories as trivial while also repeatedly regenerating simplistic escape scenarios. A recent, comprehensive study by Leipold considered the effects of orbit perturbations, Earth shadow, and a nonideal sail force model for operations in Earth orbit, yet this model also neglected the inclusion of a negative altitude constraint when considering Earth-escape trajectories.[12] A potential solution to the problem of maintaining a minimum altitude during Earth escape has recently been demonstrated, which mathematically guarantees against a collision with the central body while continuing to provide near-optimal solutions in the presence of orbit perturbations, shadow, and a nonidealized sail surface.[13] This paper follows on from Ref. 13, which concentrated on producing realistic Earth-escape solutions. We will consider the use of a solar sail for planet-centered transfers and stationkeeping. The use of locally optimal control laws for solar sailing is developed from

Received 8 June 2004; revision received 23 August 2004; accepted for publication 6 October 2004.

*Research Assistant/Lecturer, Department of Aerospace Engineering; m.macdonald@aero.gla.ac.uk.

†Professor, Department of Mechanical Engineering; colin.mcinnes@strath.ac.uk.

prior work[14] and a new control method introduced, which blends these individual control laws to provide near-optimal results.

Previously, locally optimal control laws have been used widely for low-thrust trajectory generation in which no constraint is placed on the orientation of the thrust vector, such as solar electric propulsion (SEP).[15,16] Commonly, locally optimal control laws are blended by the use of optimization techniques to set the weight functions for each control law. Therefore, the weightings are given as a function of time from the start epoch. However, the method previously outlined for solar sailing suggested that a more prudent approach would be to use the osculating orbit elements to set the weight functions of each control law.[13,14] Thus, the solution is adaptive to previously unmodeled orbit perturbations and as such provides a more robust solution to the orbit control problem while also being suitable as a potential onboard autonomous controller. A similar approach has recently been proposed by Petropoulos for SEP orbit transfers following a similar hypothesis.[17] Petropoulos uses the control laws for SEP orbit transfers and blends them to generate relatively simple transfer trajectories; this work uses a number of separate criteria to judge the importance of each control law prior to defining the blended optimal thrust vector.

The locally optimal control laws previously outlined for SEP-type transfers differ slightly from the solar-sail locally optimal control laws previously outlined. The control laws required in this paper will be derived and defined, following Refs. 13 and 14 where appropriate. We will then discuss the control method developed in order to set the weighted importance of each of the orbit elements, prior to blending the control laws. The paper will discuss the new control method for stationkeeping in previously proposed planetary solar-sail missions and investigate how such a method could enhance the science return of such missions. A complex orbit transfer at Mercury will also be presented where the main constraints are thermal and not transfer duration, which can be considered secondary in many solar-sail applications at Mercury, as will be discussed later.[2]

Locally Optimal Control Laws

The rate of change of any orbital element can be calculated and hence a locally optimal control law generated. These control laws maximize the instantaneous rate of change of the element and provide the required sail orientation in closed analytical form. Such a method provides only a locally optimal solution, which does not guarantee global optimality. In Ref. 13 the blended use of a semimajor axis control law, also known as the locally optimal energy gain control law and a radius of pericenter control law, was introduced to facilitate the generation of realistic Earth-escape trajectories. Within this paper we will evolve the work in Ref. 13 so as to incorporate control laws for the five classical orbit elements plus radius of pericenter and apocenter. The derivation of selected additional control laws is presented, which will allow derivation of all other control laws.

The variational equation of the element to be optimally altered is written in the form of Eq. (1):

$$\frac{\mathrm{d}k}{\mathrm{d}t} = \boldsymbol{f}_s.\boldsymbol{\lambda}_k \tag{1}$$

where k represents the element under consideration. The required relative perturbing force on each of the radial, transverse, and normal (RTN) axes to maximize the rate of change of k is found as a unit vector of $\boldsymbol{\lambda}_k$. Maximizing the thrust vector $\boldsymbol{f}_s$ along $\boldsymbol{\lambda}_k$ maximizes the right-hand side of Eq. (1); thus, the instantaneous rate of change of element k will be maximized. The sail control angles are defined in the standard form with respect to a sun-sail line reference frame[1] and are shown in Fig. 1. Within the sun-sail line reference frame the sun is fixed along the $-X$ axis, while the Y axis corresponds with the heliocentric velocity vector of the planet the sail is orbiting. The Z axis completes the right-hand Cartesian coordinate system.

It is required that we transpose the unit vector of $\boldsymbol{\lambda}_k$ from the satellite RTN reference frame into the sun-sail line reference frame within which the sail control angles are defined. With conversion of the unit vector of $\boldsymbol{\lambda}_k$ into the sun-sail line coordinate system, we can

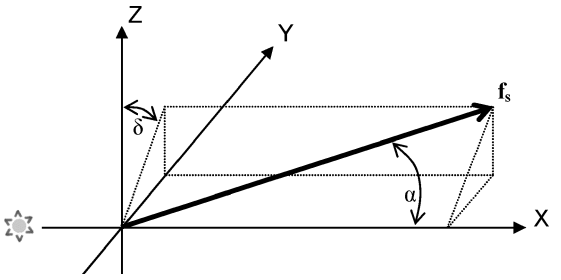

Fig. 1 Sail control angles in sun-sail line reference frame.

define $\tilde{\alpha}$ using Eq. (2). The sail clock angle is derived in Eq. (3) as

$$\tilde{\alpha} = \arccos(\lambda_x) \tag{2}$$

$$\delta = \arccos\left(\frac{\lambda_z}{\sqrt{\lambda_y^2 + \lambda_z^2}}\right) \tag{3}$$

With the derivation of the ideal force angles in the sun-sail line reference frame, a standard optimization derivative[18] is used, Eq. (4), to find the sail orientation that will maximize the sail thrust vector along the ideal force vector. The pitch angle of the ideal force vector is defined as the angle between the sun-sail line and the ideal force vector. The locally optimal sail pitch angle is thus found directly from Eq. (4) and $\tilde{\alpha}$:

$$\tan\alpha = \frac{-3\cos\tilde{\alpha} + \sqrt{9\cos^2\tilde{\alpha} + 8\sin^2\tilde{\alpha}}}{4\sin\tilde{\alpha}} \tag{4}$$

The locally optimal sail clock angle is found directly from the ideal force vector by using Eq. (3) and does not require optimization because the sail acceleration magnitude does not depend on the sail clock angle. If a negative rate of change is desired, the ideal force vector direction should be reversed, hence flipping the vector orientation before application of Eq. (4) and giving a negative rate of change.

The derivation of the semimajor axis control law is presented in Ref. 13 along with the radius of pericenter control law. The derivation of the eccentricity and radius of apocenter control laws can be derived as a simple extension of Ref. 13 and are hence not presented within this paper.

Inclination Control Law

Contrasting the semimajor axis and pericenter control laws, the rate of change of inclination depends on only the one perturbing force, the out-of-plane perturbation. Thus, the method used for locally optimal variation is somewhat different. For the locally optimal rate of change of inclination, consider Eq. (5), the variational equation of inclination,

$$\frac{\mathrm{d}i}{\mathrm{d}t} = \frac{r}{\sqrt{\mu p}}[F_R \;\; F_T \;\; F_N]\begin{bmatrix} 0 \\ 0 \\ \cos(\nu+\omega) \end{bmatrix} \tag{5}$$

From Eq. (5) we see that a switching relationship is required in order to maintain the desired sense of rate of change, positive or negative. For example, if $\cos(\nu+\omega)$ is negative we require a negative out-of-plane sail force, hence generating a positive rate of change. Conversion into modified equinoctial elements gives the switching term as $1/\tau(h\cos L + k\sin L)$; we can thus define $\boldsymbol{\lambda}_i$ in Eq. (6):

$$\boldsymbol{\lambda}_i = \begin{bmatrix} 0 \\ 0 \\ \operatorname{sgn}\left\{\dfrac{1}{\tau}(h\cos L + k\sin L)\right\} \end{bmatrix} \tag{6}$$

The sail pitch and clock angles are thus derived through conversion of $\boldsymbol{\lambda}_i$ into the sun-sail line reference frame just discussed and application of Eqs. (2–4).

Argument of Pericenter Control Law

The variational equation of the argument of pericenter, Eq. (7), is one of the few that depends on the perturbing acceleration along all three RTN axes. However, despite this, the locally optimal control law is derived in a manner similar to that of other orbit elements:

$$\frac{\mathrm{d}\omega}{\mathrm{d}t} = \frac{1}{\sqrt{\mu}}[F_R \quad F_T \quad F_N] \begin{bmatrix} -\frac{\sqrt{p}}{e}\cos\nu \\ \left(1+\frac{r}{p}\right)\frac{\sqrt{p}}{e}\sin\nu \\ -\frac{r}{\sqrt{p}}\cot i \sin(\nu+\omega) \end{bmatrix} \tag{7}$$

From Eq. (7) we can find $\boldsymbol{\lambda}_\omega$, which is given by Eq. (8) in modified equinoctial elements as

$$\boldsymbol{\lambda}_\omega = \begin{bmatrix} -\frac{(f\cos L + g\sin L)}{(f^2+g^2)} \\ \left(1+\frac{r}{p}\right)\frac{(f\sin L - g\cos L)}{(f^2+g^2)} \\ -\frac{r}{p}\left[\frac{\cot\left(2\arctan\sqrt{h^2+k^2}\right)(h\sin L - k\cos L)}{\tau\sqrt{f^2+g^2}}\right] \end{bmatrix} \tag{8}$$

Thus, the locally optimal sail pitch and clock angles are derived in a similar manner to prior control laws, with the use of Eqs. (2–4).

Blending Locally Optimal Control Laws

The rudimentary technique of blending control laws for geocentric solar-sail orbit transfers has previously been introduced.[14] The blending of control laws was further refined in Ref. 13, for the generation of realistic Earth-escape trajectories. For clarity we will very briefly review the mechanics of the actual blending process presented in Ref. 13.

The blending of control laws is accomplished by initially calculating the unit vector, in the sun-sail line reference frame, along which the force should be maximized to maximize the rate of change of each individual element being blended, obtaining a separate unit vector for each control law. We then compute the blended vector by applying Eq. (9):

$$\boldsymbol{\lambda}_b^{\text{sun}} = \frac{\sum_k W_k \boldsymbol{\lambda}_k^{\text{sun}}}{\left|\sum_k W_k\right|} \tag{9}$$

where subscript k once again represents each individual control law being blended and superscript sun denotes the vector is in the sun-sail line reference frame. From $\boldsymbol{\lambda}_b^{\text{sun}}$ we can directly define $\tilde{\alpha}$ using Eq. (2); thus, application of Eq. (4) gives the blended locally optimal sail pitch angle. The sail clock angle is derived directly from $\boldsymbol{\lambda}_b^{\text{sun}}$, using Eq. (3).

As already stated, the blending procedure outlined earlier for solar-sail applications uses the orbital elements to define the weight of each control law, rather than defining each weight as a function of time from the start epoch. Defining the weight functions by the orbital elements has additional benefits. The sail pitch and clock angles are defined as a closed loop; thus, the control system can adjust for small unforeseen orbit perturbations or perturbations that cannot currently be modeled as a result of lack of real-world knowledge such as sail wrinkles or sail degradation caused by radiation. As such, the system would potentially be suitable as an onboard autonomous controller for future sail missions. An autonomous controller is attractive as it reduces the amount of data in the uplink telecom budget by removing the need for sail control commands, which would typically be a large data set of several hundreds of points. The sail control commands could thus be replaced with the spacecraft state vectors at a given epoch.

The optimality of the blended system depends heavily on the weight functions applied in gaining the blended locally optimal thrust vector. In Ref. 13 the weight functions were defined by a series of simple exponential relationships. However, in attempting to create a more complex and robust control system for orbit transfers and stationkeeping applications we require an evolution of the derivation and calculation of the weight functions.

Accessibility and Deficit Blending

The accessibility and deficit (A^nD) blending method seeks to give each individual control law a relative importance before defining the final weight functions and thus the blended control vector. The deficit of each element from the final target value is considered. Additionally, the efficiency or accessibility of any attempt to alter an orbital element is considered, thus avoiding inefficient use of the sail such as in prolonged periods of high pitch.

The deficit is found not by consideration of each element's value, but instead by estimation of the time required to attain the target value using the locally optimal control law. We compute $\boldsymbol{\lambda}_k^{\text{sun}}$, thus allowing the locally optimal pitch and clock angle for control law k to be found. With the locally optimal pitch and clock angles calculated, we can thus calculate the sail perturbation vector in sun-centered coordinates, by using Eq. (10), as

$$\boldsymbol{f}_k = \begin{bmatrix} \cos\alpha_k \\ \sin\alpha_k \sin\delta_k \\ \sin\alpha_k \cos\delta_k \end{bmatrix} \tag{10}$$

Equation (10) is then converted back into satellite RTN axis in order to calculate $\mathrm{d}k/\mathrm{d}t$, the rate of change of element k. To find $\mathrm{d}k/\mathrm{d}t$, we must find the magnitude of the sail perturbation vector using Eq. (11) to correct sail acceleration caused by the locally optimal sail pitch angle:

$$a_s = a_{s_c}\cos^2\alpha_k \tag{11}$$

With knowledge of the locally optimal rate of change of element k, the current value of k, and the target value of k, it becomes a simple matter to estimate the time required to attain the target value assuming a constant rate of change. Repeating this process for each control law being blended allows us to normalize the time required with respect to the greatest time. Thus, each control law gains a score between zero and one for the corresponding deficit, with zero meaning the element has attained its target value and one that it is the furthest, or has the greatest deficit, from its target value.

The deficit of an element can appear excessively high if the corresponding locally optimal pitch angle is high, which results in a low rate of change and thus gives a high deficit score to an element that will poorly use the sail. We thus consider the accessibility of control law k by consideration of the corresponding optimal pitch angle. From Eq. (11) we see that as the pitch angle is increased the corresponding sail acceleration drops off as the cosine squared. The accessibility score is found by calculating the cosine squared of the optimal pitch angle for each control law and normalizing with respect to the largest. Hence, the control law that best utilizes the sail acceleration gains a score of one, while the most inefficient gains a low score. Using the A^nD blending method we can select the weight functions based not only on need, but also on an opportunistic level. The deficit score gives the highest score to the element furthest from its target value, whereas the accessibility score gives priority to the element that most efficiently uses the sail. Combination of the two scores provides the weighted relevance of each control law; however, the method of combining the two scores must itself be carefully considered and rationalized. Multiplying the accessibility and deficit scores results in a low total score should either score be low. However, it has been found that if an element has low accessibility for a given direction of change, say negative, this is because the orbit alignment about the planet and with respect to the sun is typically close to optimal for the opposite direction of change. As a result of this, if an element has low accessibility and high deficit, then multiplication of the two scores results in an increase in the deficit. It is thus found that even though the accessibility is low we cannot ignore the element. Addition of the two scores results in a low accessibility and high deficit scenario receiving a middle

of the range score and was thus found to offer a better solution. The final A^{n}D score is thus found by addition of the two individual scores.

The final weight functions are found by multiplying an individual element A^{n}D score by a constant. For example, as will be seen later, the GeoSail mission primary requirement is to rotate the orbit argument of pericenter. Thus an additional importance is placed on this element, and it is multiplied by a larger constant. Elements that are not being blended are multiplied by zero to remove them from consideration, and elements of less importance are multiplied by smaller weights. The use of weights allows the control system to be fine-tuned to increase optimality. The selection of appropriate constants is intuitive and typically follows the mission goals, such as seen for the GeoSail mission. However, an initial guess can be gained by using the A^{n}D scores only, before then introducing the constants to improve optimality if it is unclear which orbital elements should be focused on.

Orbit Transfer's Using A^{n}D Blending

The generation of solar-sail planet-centered orbit transfers are perhaps of limited purpose. For instance, lengthy Earth-escape spirals at the beginning of a heliocentric mission should be eliminated by the launch vehicle whenever possible. If however the sail is the primary form of propulsion, then during a reconnaissance or sample and return mission the sail must be utilized to correctly deliver the science payload to the target orbit about the destination body. Much prior work that has claimed to generate capture trajectories has simply been escape trajectories integrated over a negative time span. However, such an approach does provide a suitable approximation to obtain the required timescale of any capture trajectory and is thus suitable for early mission analysis studies.

Only a few solar-sail planet-centered orbit transfers have been previously published primarily because of the significant difficulty of generating trajectories that are optimized over numerous revolutions. A rudimentary transfer from geostationary transfer orbit (GTO) to the original GeoSail mission orbit of 10×30 Earth radii was generated using locally optimal control laws.[14] A recent doctoral thesis used extremal steering strategies for simulation and optimization of Earth–moon transfer trajectories using solar sailing.[19] This work resulted in the solution of a weak stability boundary problem and generated realistic transfer trajectories from GTO to bound lunar orbit. One of the few other published planet-centered solar-sail transfer trajectories, other than lunar flybys, which are not actual orbit-to-orbit transfers, was in a 1977 study.[20,21] This study developed a computer program to calculate optimal planet-centered trajectories; however, only one orbit-to-orbit transfer was generated as it was found that the coding required a very good initial guess before a solution was found and that eccentricity convergence was difficult when the target eccentricity was low. Transfer to subescape points presented no convergence difficulties; however, orbit transfers were much more difficult, and the authors were unable to generate more than one complete trajectory within the time frame of the study.

It is the experience of the authors that although planet-centered orbit transfers are of only limited purpose, when they are required the primary cost function is seldom time. For example, the primary cost function for sail operations at Mercury is typically thermal and avoidance of passage near the subsolar point. During a recent Mercury sample and return mission study,[2] it was found that the surface thermal conditions were such that a lander could only survive at key specific times of the Hermian year. It was also found that the optimal Earth–Mercury transfer and subsequent capture spiral result in arrival of the lander at an inappropriate time for landing. Thus, we require the lander to wait in Mercury orbit until the surface thermal conditions are suitable. The optimal orbit for the sail to enter while waiting for the surface conditions to become suitable was found to be the Mercury-forced sun-synchronous orbit,[12,22–24] hence minimizing thermal loads on the sail and its systems. Thermal requirements thus necessitate an orbit-to-orbit transfer from the sun-synchronous orbit to the low-circular near-polar orbit for deployment of the lander. The primary cost function of this transfer is not time as the arrival time is fixed, and the transfer is necessitated by a need to wait for the correct surface conditions.

Mercury-Forced Sun-Synchronous Orbits

A Mercury solar-sail trajectory model including solar gravity effects and Mercury J_2 was created. The solar-sail force model utilizes a standard optical model,[1] whereas the sun is modeled as a uniformly bright finite disk. The eccentric nature of Mercury's orbit also makes it important that we accurately model the true sail-sun distance, hence modeling the true variation of sail acceleration through the Hermian year. Furthermore, the trajectory model also considers and distinguishes between umbra and penumbra shadow on the sail surface. Modified equinoctial elements are used in the equations of motion, which are propagated by using an explicit, variable step size Runge–Kutta formula, the Dormand–Price pair, with relative and absolute error tolerances of 10^{-9} ensuring minimal truncation error.[25]

The close proximity of Mercury to the sun means that even a relatively modest level of sail performance can provide a significant thrust vector. Mercury has a reciprocal of flattening over 18 times that of Earth, with a J_2 value of only 60e-6, although the reciprocal of flattening is often mistakenly quoted as being infinite. Thus, once in orbit about Mercury it is not possible to create a natural sun-synchronous orbit; a supplemental thrust vector is required to replace the oblateness utilized at Earth. Leipold and Wagner showed that this supplemental thrust could be provided by a modest solar sail in a highly elliptical polar orbit,[24] consequently allowing the spacecraft to maintain station at or near to the solar terminator of Mercury. As such, the thermal loading caused by reflection and reradiation from Mercury's surface is significantly reduced, while the severe thermal cycling encountered by numerous passes through the shadow cone is also eliminated. It is considered that the optimal remote sensing orbit places the spacecraft at a small offset from the solar terminator, rather than directly overhead as the low sun angles near the terminator on the dayside of the planet allow high topographic discrimination in near-constant illumination conditions. Finally, because of Mercury's rotational period:orbital period, 3:2 resonance, the sun-synchronous polar orbit allows complete surface coverage in only 88 days. However, because of the optimal orbit offset from the solar terminator it is necessary to remain in orbit for 176 days to acquire full surface visual coverage and dual coverage in other spectrums. It is thus clear that such a reconnaissance orbit is of great potential scientific use and worthy of study.

Recreating the trajectories published by Leipold and Wagner it is found that the orbit is an unstable equilibrium point. It has been shown previously that the ascending node angle cannot be varied without also altering the argument of pericenter angle.[26] It was similarly noted by Leipold and Wagner that the argument of pericentre experienced a long period oscillation caused by the sail thrust vector. Over short timescales the small variation in argument of pericenter results in only small variations in semimajor axis and eccentricity. However as the argument of pericentre reaches the peaks and troughs of its long period oscillation, the nominal pericenter altitude of 200 km varies as low as 70 km and rises as high as 400 km, before collision with the Hermian surface. Collision typically occurs around day 100–140 from the initial start epoch, depending on initial conditions. It thus becomes clear that although the optimal science orbit has a very low pericenter we require either an active sail to achieve this, as will be discussed later, or an initially greater altitude.

We determine the allowed sun-synchronous orbits for a given sail characteristic acceleration, defined as the acceleration experience by an idealized, 100% reflective sail at 1 astronomical unit, through analysis of the variational equation of motion of the ascending node angle[27] [Eq. (12)]:

$$\frac{\mathrm{d}\Omega}{\mathrm{d}t} = \frac{F_N r \sin(\omega + \nu)}{\sqrt{\mu_M a(1-e^2)}\sin i} = \frac{F_N r}{\sqrt{\mu_M p}} \frac{\sin(\omega + \nu)}{\sin i} \tag{12}$$

Following Leipold and Wagner,[24] we can integrate Eq. (12) over one orbit period, assuming inclination, semilatus rectum, and argument

of pericenter are constant over the orbit period and the sail orientation is constant over one orbit revolution and directed normal to the orbit plane; that is, $\alpha = 0$ deg for orbits along the terminator and $\alpha = 10$ deg for orbits offset from the terminator by 10 deg. Changing the integration variable from time to true anomaly allows the derivation of Eq. (13):

$$\Delta\Omega\Big|_{\omega+\nu=0}^{\omega+\nu=2\pi} = \frac{F_N p^2}{\mu_M \sin i} \int_{\omega+\nu=0}^{2\pi} \frac{\sin(\omega+\nu)}{(1+e\cos\nu)^3}\,\mathrm{d}\nu \tag{13}$$

The precession of the node can thus be determined by using the orbit period as given in Eq. (14) as

$$\dot{\Omega} = \frac{\sqrt{a}\,F_N(1-e^2)^2}{2\pi\sqrt{\mu_M \sin i}} \int_{\omega+\nu=0}^{2\pi} \frac{\sin(\omega+\nu)}{(1+e\cos\nu)^3}\,\mathrm{d}\nu \tag{14}$$

Extending the analysis performed by Leipold and Wagner,[24] we can generate contours of the potential sun-synchronous orbits for a given sail acceleration or offset angle from the solar terminator, thus enabling rapid assessment of different potential scenarios. Analysis of Eq. (14), with $\omega = \pi/2$ or $3\pi/2$ and setting $i = \pi/2$, such that $\sin i = 1$, allows derivation of Eq. (15):

$$a = \left[\frac{F_N(1-e^2)^2}{2\pi\dot{\Omega}\sqrt{\mu_M}} \int_0^{2\pi} \frac{\cos\nu}{(1+e\cos\nu)^3}\,\mathrm{d}\nu\right]^{-2} \tag{15}$$

The required rate of change of ascending node angle for a sun-synchronous orbit is found to be the specific angular momentum of Mercury with respect to the sun divided by the square of the Mercury–sun distance. Thus, the required rate of change of ascending node angle varies between 1.28×10^{-6} and 5.57×10^{-7} rad s^{-1} depending on Mercury's position. However, as Mercury orbits the sun the sail acceleration varies as the inverse square of the solar distance; thus, the induced rate of change of ascending node will vary similarly, as required. Thus, no alteration in the orbit is required during the Hermian year as was also found by Leipold and Wagner.

Solving Eq. (15) for a given eccentricity allows the corresponding semimajor axis for any given sail acceleration level to be determined. For example, the orbit defined previously by Leipold and Wagner for utilization within a future science mission was for a sail with characteristic acceleration 0.25 mm s^{-2} at zero offset from the solar terminator. Pericenter altitude was defined as 200 km, and apocenter altitude was quoted as approximately 6350 km. We find that the actual idealized value is 6293.63 km for such a scenario. Extending the analysis for a sail characteristic acceleration 0.25 mm s^{-2}, we see in Fig. 2 a plot of pericenter altitudes vs apocenter altitudes for a range of solar terminator offset angles. Above a 50-deg offset angle from the solar terminator, the orbit begins to intersect the shadow cone; we recall that for an orbit offset from the solar terminator we require to maintain the sail force vector normal to the orbit plane, and as such the fixed sail pitch angle equals the nominal offset angle. Figure 3 shows a plot of pericenter altitudes vs apocenter altitudes for a range of sail accelerations and orbits with solar terminator offset angles of 0 and 10 deg; we note that the 0.25 mm s^{-2} contours correspond to the 0- and 10-deg contours shown in Fig. 2. We see in Fig. 3 that the increased sail accelerations allow for the apocenter to be lowered for a given pericenter value, whereas the increase in solar terminator offset angle requires an increase in apocenter altitude for

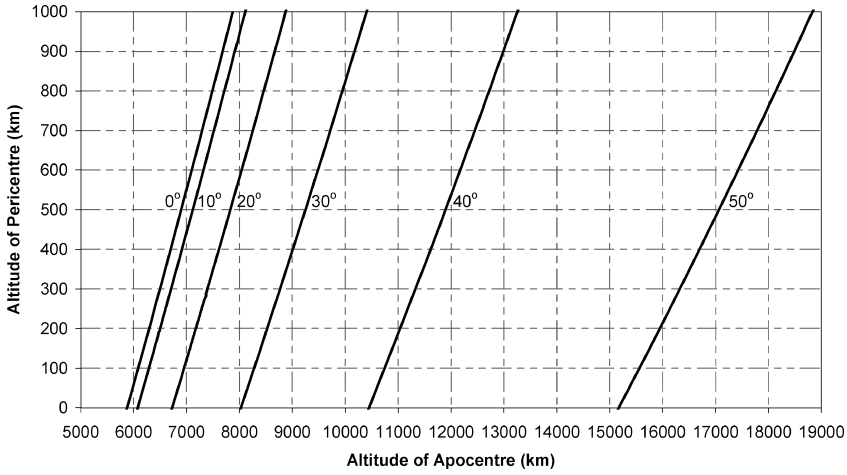

Fig. 2 Pericenter vs apocenter contours for $a_{s_c} = 0.25$ mm s^{-2} forced sun-synchronous orbits, at a range of offset angles from the solar terminator.

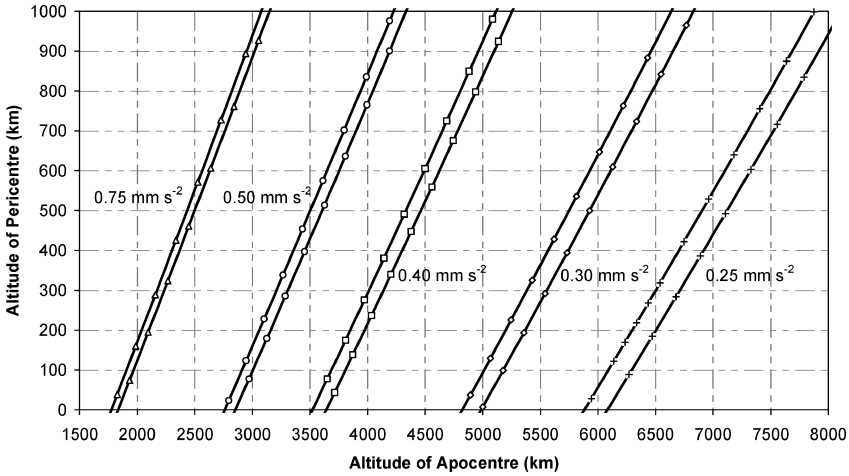

Fig. 3 Pericenter vs apocenter contours for orbit planes at 0- and 10-deg offset from solar terminator at a range of sail accelerations.

a given pericenter value. We note that the orbits defined in Figs. 2 and 3 correspond to the required actual thrust vector and have not been corrected for an imperfect sail surface.

For a fixed-sail orientation we select an increased pericenter altitude of 500 km; noting that Leipold and Wagner first suggested a pericenter altitude of 600 km before later reducing this to 200 km (Ref. 22). The sail orbit is displaced from the terminator by 10 deg. We see from Eq. (15) and Figs. 2 and 3 that the apocenter altitude is thus 7109.9 km, for a sail characteristic acceleration of 0.25 $\text{mm} \cdot \text{s}^{-2}$. Note, sail characteristic acceleration is fixed at 0.25 $\text{mm} \cdot \text{s}^{-2}$ for the remainder of this paper when discussing sail operations at Mercury. Using the trajectory model just discussed, we can propagate a 180-day simulation for a forced sun-synchronous orbiter with pericenter over the northern geographical pole. Start epoch at 05 July 2010 gives an initial ascending node angle of 54.5 deg. The ascending node angle varies from this initial value to 360 deg and back up to approximately 54.5 deg after one Hermian year. The rate of change of ascending node varies throughout the Hermian year, as expected, thus maintaining a separation angle from the solar terminator of approximately 10 deg. The orbit inclination remains within +0.45 and −0.27 deg of 90 deg; similarly, the argument of pericenter varies minimally. It is found that both the pericenter and apocenter altitudes vary considerably from the initial values quoted. Large variations could potentially impact the science goals of the mission, and as such active sail control could potentially be used to minimize pericenter altitude variation, while also lowering the pericenter altitude. Such an active sail control system will be discussed later within this paper.

The 180-day propagation terminates on 01 January 2011 with the corresponding orbiter position elements defined in Table 1. We note that the final pericenter altitude is 361 km above its nominal value. Inclination and argument of pericenter are both close to their nominal values, while the ascending node angle places the orbiter ground track approximately 10.3 deg ahead of the solar terminator.

We can use the elements defined in Table 1 as starting conditions for an orbit transfer to a south-pole pericenter orbit. Such a transfer would potentially enable high-resolution mapping of the entire surface of Mercury with a single spacecraft. Leipold et al. proposed using two spacecraft for such 100% coverage.[23]

Transfer Between Sun-Synchronous Orbits by Using A^{n}D Blending

A direct transfer from a north-pole pericenter to south-pole pericenter forced sun-synchronous orbit is relatively simple. The argument of pericenter and ascending node angles must be rotated through 180 deg, while the nominal value of all of the other elements remains unaltered. However, a direct and simple transfer would require the orbiter to pass directly over the subsolar point and through the planetary shadow cone. We thus optimize the transfer orbit such that the orbiter does not pass through the planetary shadow cone at any point of the transfer. The primary optimization cost function hence becomes spacecraft thermal constraints rather than a minimum time transfer.

Using the orbit elements in Table 1 as the initial conditions for the orbit transfer, we define the target elements in Table 2. Several potential strategies can be adopted to eliminate planetary shadow from this transfer. The ascending node angle could be rotated very rapidly, or the orbit velocity could be reduced to approximately zero and then the direction reversed on a parabolic orbit at a large orbit radius. However, this second option would require the orbit energy to approach zero and would require a very high level of navigation accuracy. Alternatively, the adopted strategy was to raise the orbit energy and circularize the orbit, allowing the planet to rotate rapidly beneath the orbiter. The use of a circular orbit also much simplifies the transfer, as the argument of pericenter can be selected as eccentricity rises again, rather than actually rotating the orbit through 180 deg. The targeting of a continually varying ascending node adds an additional complication to the optimization, but we find that the A^{n}D blending method handles such a condition well.

Table 1 Orbit elements after 180-day forced sun-synchronous orbit

Orbit element	Value
Semimajor axis	6258.2 km
Eccentricity	0.47
Altitude of pericenter	861.2 km
Altitude of apocenter	6775.8 km
Inclination	90.26 deg
Argument of pericenter	89.84 deg
Right ascension of ascending node	75.11 deg
True anomaly	228.44 deg

Table 2 Target orbit elements for forced sun-synchronous orbit with south-pole pericenter

Orbit element	Value
Semimajor axis	6244.65 km
Eccentricity	0.53
Altitude of pericenter	500.0 km
Altitude of apocenter	7109.9 km
Inclination	90.00 deg
Argument of pericenter	270.0 deg
Right ascension of ascending node	($\Omega_{\text{sun}} + 10^\circ$) deg +180 deg from N-pole value
True anomaly	228.44 deg

The transfer trajectory is split into eight phases and propagated using the trajectory model already discussed within this paper. The first phase of the trajectory raises the orbit energy using the semimajor axis control law exclusively for approximately 27 days. Subsequent phases have similar intermediate aims, which all contribute towards the final complete trajectory. For example, the purpose of the second phase is the reduction of eccentricity to zero, while also targeting an ascending node value that aligns the orbit correctly for passage of the ascending node/solar terminator offset angle through the 90-deg mark, when avoidance of the shadow cone is critical. The weight by which the A^{n}D score is multiplied is determined by the relative importance of each element during that particular phase of the trajectory; hence, in phase 2 the eccentricity and right ascension angle have high weights, and the semimajor axis weight is low. Additionally, at certain times the target eccentricity is set to zero, rather than that given in Table 2; this was found to reduce transfer time, which, although not the primary cost function of the transfer, remains of critical importance. Furthermore, at certain times the control laws are not allowed to automatically determine which direction they should be driving the orbit; instead, they are forced to always increase a certain element irrespective of current and target values. For example, the ascending node angle is always increased and never decreased; this has a slightly different effect from altering the target value, as the A^{n}D score is affected in a different way but is done for similar reasons. Selection of such strategies is through engineering judgment.

Analytical analysis of Mercury, sun, and spacecraft position vectors can be used to confirm the entire transfer trajectory is shadow free. We define the spacecraft shadow parameter in Eq. (16) as

$$\varsigma = -\frac{|\boldsymbol{r}_{\text{sat}} \times \boldsymbol{r}_{\text{sun}\to\text{sat}}|}{|\boldsymbol{r}_{\text{sun}\to\text{sat}}|}\text{sgn}(\boldsymbol{r}_{\text{sat}} \cdot \boldsymbol{r}_{\text{sun}\to\text{sat}}) \tag{16}$$

The critical shadow parameter for penumbra conditions is defined in Eq. (17) as

$$\varsigma_p = |\boldsymbol{r}_{\text{sat}}| \sin\left[\arcsin\left(\frac{r_M}{|\boldsymbol{r}_{\text{sat}}|}\right) + \arcsin\left(\frac{r_{\text{sun}} - r_M)}{|\boldsymbol{r}_{\text{sun}\to M}|}\right)\right] \tag{17}$$

We note that the umbra critical shadow parameter is found by replacement of the negative Mercury radius term in the second arcsine expression with a positive Mercury radius. We concentrate on penumbra shadow however as this ensures the sail remains within full sunlight at all times. If the magnitude of the spacecraft shadow parameter is greater than the magnitude of the penumbra critical shadow parameter, then the spacecraft is in complete sunlight on the night side of the planet, and if the shadow parameter is less than

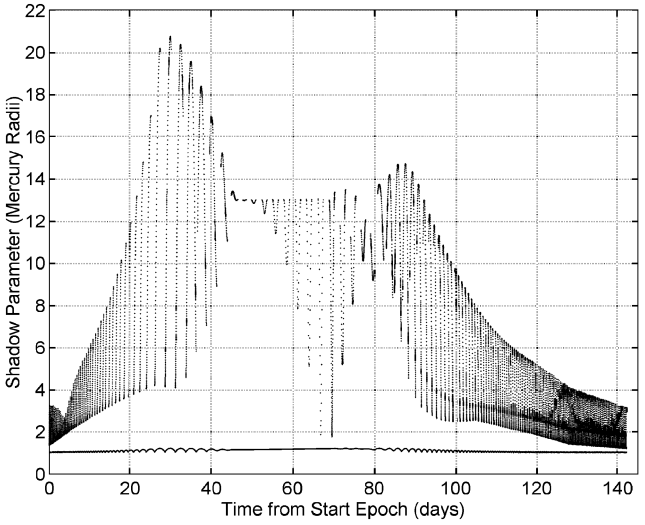

Fig. 4 Spacecraft shadow parameter (night side of planet only) and penumbra critical shadow parameter.

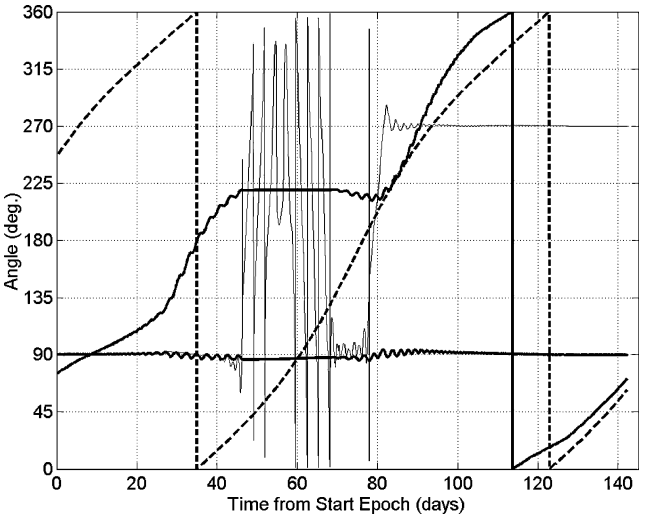

Fig. 5 Right ascension of orbiter (——, starting at ∼54 deg), right ascension of target solar terminator ground track (- - - -), argument of pericenter (——) and inclination (——, starting at 90 deg and ending at 90 deg).

zero, then the spacecraft is on the day side of Mercury and thus in complete sunlight. Postprocessing the spacecraft shadow parameter output vector from the trajectory analysis, we can remove the terms that correspond to the spacecraft being on the day side of the planet. Figure 4 shows the penumbra critical shadow parameter throughout the transfer trajectory, and it is seen that at all times when the spacecraft is on the night side of the planet the spacecraft shadow parameter is greater than the penumbra critical shadow parameter; thus, we can confirm the trajectory is entirely shadow free.

Figure 5 shows the orbit argument of pericenter and inclination angles, which are shown to converge with their target values, while the right ascension angle is seen to terminate 10 deg ahead of the solar terminator. Finally, Fig. 6 shows the altitude of pericenter and apocenter throughout the 142.3-day trajectory. We see that the orbit eccentricity peaks at day 30, before an extended period where eccentricity is very low, which corresponds with the rapid variations in argument of pericenter angle in Fig. 5. Figure 6 shows that both pericenter and apocenter converge well with the target values, with all of the orbit elements reaching convergence with Table 2 values on day 142 of the simulation.

The transfer trajectory created using A^{n}D blending requires numerous rapid sail slew maneuvers. Furthermore, the time optimality

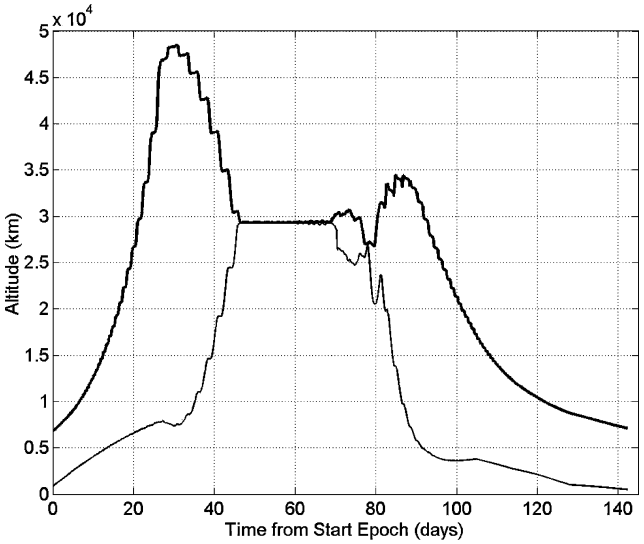

Fig. 6 Instantaneous altitude of pericenter and apocenter during transfer trajectory.

of the transfer at approximately 142 days is difficult to evaluate; however, we recall that this was not the primary cost function of the transfer. The transfer trajectory is constrained by spacecraft thermal considerations and is verified as being shadow free. Hence, we can state that it is possible to generate a shadow-free transfer trajectory between a north-pole pericenter forced sun-synchronous orbit and a south-pole pericenter orbit. Moreover, we can state that the use of A^{n}D blending has enabled such a transfer to be generated much easier than would be possible with conventional optimization tools.

Forced Sun-Synchronous Orbit with Active Sail Control by Using A^{n}D Blending

One of the significant attractions of using a solar sail to generate a forced sun-synchronous orbit is the lack of sail control requirements. The sail pitch angle is constant at all times through the orbit, and as such sail attitude control could be maintained by mostly passive methods. If the sail were used to deliver the payload into Mercury orbit, then an active sail control system would be required for the Earth–Mercury transit and the capture spiral. However, if the sail is delivered to Mercury by a chemical, electric, or combination of systems, then it could be deployed in Mercury orbit, allowing a relatively small, simple, and low-cost solar sail to be used. Such an approach would appear to be the best approach for a near-term, low-risk mission, as sail capture maneuvers typically require a high sail slew rate capability and increase mission risk, meaning that such a mission requires more advanced sail technology. We note, however, that the polar nature of the target orbit in this sun-synchronous scenario actually allows a fixed-sail pitch of arctan $(1/\sqrt{2})$ to be utilized while spinning the sail clock angle through 360 deg each orbit. Such a fixed-pitch capture trajectory can actually be accomplished in a marginally shorter time than the locally optimal steering strategy requires. Both fixed pitch and locally optimal trajectories are shadow free.

The primary requirement of an active sail control system for a forced sun-synchronous orbit is clearly that the ascending node angle is rapidly rotated. It is logical therefore to investigate the use of the ascending node angle control law exclusively. The control law autonomously selects whether to increase or decrease the ascending node angle based on the current and target values. We find, however, that the variation of pericenter and apocenter altitude through a single Hermian year is considerably more than a fixed-sail pitch over two Hermian years. This is a direct result of an increase in the amplitude of the long period oscillation of the argument of pericenter, as discussed earlier. We also find that the right of ascension angle follows the solar terminator much more poorly as a direct result in the substantial variations in orbit size and shape. The inclination angle varies by as much as $+5$ and -6 deg from the nominal value

of 90 deg. It is thus evident that an active sail control system must consider more than just the right ascension control law as a result of the unstable nature of the orbit.

It is found that in the fixed-sail-pitch scenario the orbit offset from the solar terminator is not a constant, instead varying from plus 10 deg, the nominal value, to as low as +3 deg and as high as +14 deg from the terminator. With such wide variations in the offset angle, the surface illumination conditions would not be constant. We thus require the active sail control system to provide a much more constant solar terminator offset angle and hence a much more constant surface illumination angle. It was also mentioned earlier than an active sail control system could potentially allow a reduction in pericenter altitude. Such a reduction increases surface resolution imaging for science data. Accordingly, an active sail control system for a forced sun-synchronous orbit is beneficial if it provides an improvement in surface illumination consistency and an increase in surface image resolutions, without any adverse effects on other orbit elements and parameters.

When we consider the fixed-sail-pitch scenario, the offset angle from the solar terminator, the orbit eccentricity, and semimajor axis each vary considerably. It is thus logical that when first attempting to generate an active sail control scenario we would attempt to control only these orbit elements. It was found, however, that when we control only these elements that the orbit inclination and argument of pericenter now vary significantly more than in the fixed-sail-pitch scenario, primarily because of the coupling in the out-of-plane perturbation terms. As a result of these initial findings, it is apparent that an active sail control system must control orbit size and shape, while also considering the exact orbit plane location rather than just its ascending node angle.

When propagating stationkeeping trajectories using the A^nD blending method, we set the sail pitch angle at given discrete time steps; typically, these time steps are equal to or less than a quarter of the nominal orbit period. The pitch and clock angle are set by the current orbital elements without any forward-looking considerations through the duration of the time step. The use of discrete time steps has two objectives; primarily in the forced sun-synchronous scenario, it is implemented in order to reduce computation costs, as the variable step-size integrator has a tendency to take very small step sizes when the current and target elements are close together. By fixing sail pitch for a given period of time, the integrator can propagate the orbit, while maintaining calculation accuracy without readjusting the sail at very small time steps. Although the sail pitch is set in discrete time steps, the integrator is still variable step size and typically takes many steps during each discrete pitch angle setting. The use of discrete sail pitch angle settings also has the effect of removing the potential requirement for multiple large angle slews in a very short period of time. Furthermore, if the discrete settings are significantly far apart the time required to slew the sail between settings can become significantly shorter than each discrete pitch time step; hence, sail slew rate effects are minimized within the trajectory simulation. Such a scenario is investigated later within this paper, when we analyze A^nD blending applications within the GeoSail mission framework.

The use of active sail control to generate a forced sun-synchronous orbit at Mercury allows the pericenter altitude to be significantly lowered. It was found that pericenter could be taken below 100 km and easily maintained within a narrow range of altitudes. It was felt, however, that altitudes below 100 km were undesirable, partly for science data acquisition and that in order to maintain very low pericenter values within safe bounds we were required to relax control of other orbit elements. As such, we define the nominal forced sun-synchronous orbit as 100-km pericenter altitude and 7500-km apocenter altitude, with ground track displaced 10 deg ahead of the solar terminator. Using the constants detailed in Table 3, we obtain the final weight functions used to gain a forced sun-synchronous orbit at Mercury with A^nD blending setting sail pitch and clock angle once per hour. It was found that the control method had a tendency to bring the ascending node angle 10 deg ahead of the terminator and then allow it to drift backwards before then acting to drive it back toward its nominal value. As a result, the average offset angle

Table 3 Constant weights by which A^nD score is multiplied to gain final weight functions

Control law weight	Constant factor on A^nD score
$W_e =$	8
$W_a =$	6
$W_i =$	20
$W_\omega =$	4
$W_\Omega =$	35
$W_{r_p} = W_{r_a} =$	0

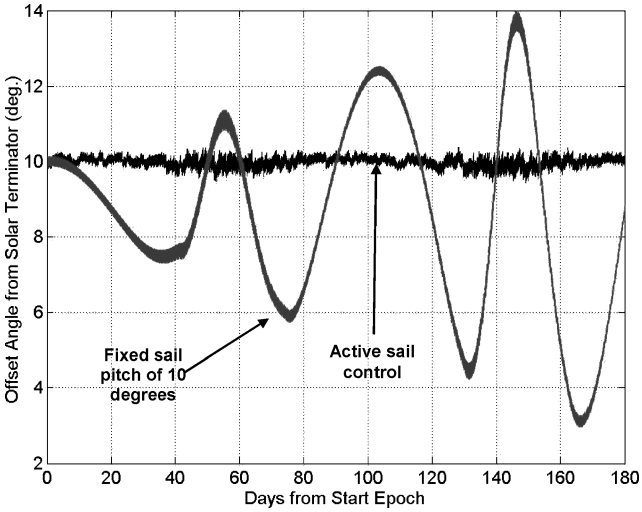

Fig. 7 Orbiter/solar terminator offset angle, fixed and active sail control.

from the solar terminator tended to be less than 10 deg; we therefore set the target offset angle at 10.25 deg, forcing the ascending node ahead of its nominal value and then allowing it to drift backward through the nominal value, hence gaining an average offset angle much closer to the nominal, as seen in Fig. 7. We also see in Fig. 7 that the offset angle is maintained within very tight bounds at certain times of the Hermian year, for example, in days 0–20 and 80–100 the offset angle is maintained with ±0.2 deg. Yet at other times the offset angle spikes at values as much as 0.5 deg away from the nominal; such events are found to correspond with Mercury's perihelion passage and the significantly increased levels of solar radiation pressure acting on the sail. The ability of the A^nD blending method to maintain orbit control during such large fluctuations in orbit perturbations illustrates the self-adaptive nature of the control system. We recall that solar radiation flux varies from four times Earth values at Mercury aphelion to just over 10 times at Mercury perihelion, a variation of 250% in orbit perturbation magnitude during each Hermian year. We note that the maximum recorded sail pitch angle during the active sail control trajectory show was 70 deg; thus, although the active sail provides excellent orbit control, it would require an agile sail.

Figure 7 shows the offset angle from the solar terminator for a fixed-sail-pitch angle of 10 deg and for an active sail control. As stated earlier, it is seen that the fixed-pitch sail has a much larger variation in offset angle than an actively controlled sail, which thus provides a much more consistent level of surface illumination for science data acquisition. We see in Fig. 8 the displacement in pericenter and apocenter from their nominal values for fixed-sail pitch and an active sail control. The active sail significantly reduces variation in orbit size and shape, with pericenter varying by 40 km and apocenter by less than 100 km. Hence the active sail control would provide a much more constant surface resolution during science data acquisition. A final consideration with the use of an active sail control system is that it should not adversely affect the orbit elements that previously were noted to vary little with a fixed-sail control system. We find that both the fixed-sail pitch and active sail

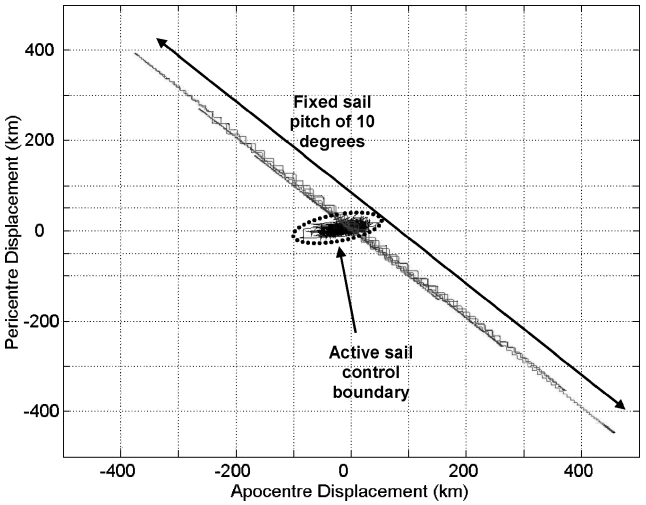

Fig. 8 Displacement of pericenter and apocenter from nominal values, fixed and active sail control.

control system result in only very small variations in inclination and argument of pericenter.

GeoSail Orbit Control by Using A^{n}D Blending

The use of an active sail control for forced sun-synchronous orbits at Mercury has been shown to significantly improve orbit uniformity. However, the short orbit period necessitates many rapid sail slew maneuvers. The GeoSail mission utilizes a much larger orbit at Earth, with a nominal period of just over four days. The GeoSail mission uses an orbit with a sun-pointing perigee at 11 Earth radii and apogee at 23 Earth radii. The orbit is positioned within the ecliptic plane, and the sail pitch angle is fixed at 0 deg; thus, the natural inversions of the radial and tangential thrust vectors about the orbit, as a result of the orbit plane location, result in a secular variation of the argument of perigee, whereas all other orbit elements experience zero secular variation. By correctly selecting the sail acceleration, we can match the rate of change of argument of perigee to that of the Earth/sun line; hence, maintain an orbit with apogee inside the Earth's magnetotail.[28] An inertially fixed orbit on this scale has apogee within the magnetotail once per year; rotation of the argument of perigee allows continuous, year-round observations of the magnetotail with a single spacecraft.[28]

The A^{n}D blending method for active sail control is considered within the GeoSail mission for a purpose similar to that for which it was considered within the Mercury forced sun-synchronous orbiter mission; that is, whereas the GeoSail orbit is a more naturally stable scenario, we consider the use of an active sail control system to maintain a more precise orbit than would otherwise be attained by a fixed-sail-pitch scenario, with the corresponding oscillations in orbit elements. However, we additionally consider the application of a fixed upper limit to the allowed sail pitch angle. The imposition of an upper pitch angle means that we can expect much smaller sail slew angles between discrete sail pitch settings. It also simplifies spacecraft design if the solar aspect angle is more constant. We set the duration of each discrete sail pitch angle as one day, just under a quarter of the nominal orbit period. It was found that using a single set of weights on the A^{n}D scores we could maintain good orbit control down to an upper pitch angle of 15 deg. Reduction of maximum pitch to 10 deg was found to be overly restrictive, and the control system required an increase in sail acceleration. The required sail acceleration is determined by consideration of the orbit size and shape as defined in Ref. 28; the required sail characteristic acceleration is 0.0999 mm s^{-2}.

The Earth-centered trajectory model uses modified equinoctial elements in the equations of motion; the perturbational equations of motion are propagated using an explicit, variable-step-size Runge–Kutta formula, the Dormand–Price pair with relative and absolute error tolerances of 10^{-9} ensuring minimal truncation error.[25] The solar sail force model uses a standard optical model,[1] whereas the sun is modeled as a uniformly bright finite disk. The true sail-sun distance is determined, correcting for the eccentricity of Earth's orbit in order to correctly quantify the sail acceleration. The trajectory model includes third-body gravity effects caused by both the Moon and the sun, while modeling the Earth as a nonspherical body up to and including the 18th-order harmonics. Umbra and penumbra shadow from the Earth and the moon are also included within the trajectory model.

Using the constant weights detailed in Table 4, we obtain the final weight functions used to generate a GeoSail orbit with active sail control, setting sail pitch and clock angle once per day. We note that the factor by which the argument of perigee is multiplied by is much larger than the other control laws. The value of each factor reflects the importance of the orbit element. Similar to the Mercury-forced sun-synchronous orbit, we find it is beneficial to target the primary orbital element, the argument of perigee is this case, ahead of the nominal value. Thus, the argument of perigee is targeted 0.2 deg ahead of the Earth–sun line.

The maximum sail pitch angle allowed is 15 deg; thus, if the blended locally optimal pitch angle is greater than 15 deg the pitch angle is set as 15 deg, with the clock angle allowed to take any value between 0 and 360 deg. Similar to the Mercury-forced sun-synchronous scenario, the sail control angles are set by consideration of only the current orbit elements, and no forward-looking considerations are taken. We see in Fig. 9 the displacement of perigee and apogee from the nominal values of 11 and 23 Earth radii, respectively, for the fixed-sail-pitch and active sail control scenarios. It is found that the active sail control scenario using A^{n}D blending to select the sail control angles reduces the variation in orbit perigee and apogee, thus providing a much more consistent orbit shape and size. The radius of perigee is seen in Fig. 9 to be centered on a value of approximately 10.8 Earth radii, rather than the nominal value of 11 Earth radii. If desired, the target perigee could be raised to 11.2 Earth radii; thus, the orbit would shift toward the nominal GeoSail orbit in a similar manner to that used for accurate targeting of the argument of perigee. We note, however, that this is a magnetotail

Table 4 Constant weights by which A^{n}D score is multiplied to gain final weight functions

Control law weight	Constant factor on A^{n}D score
$W_{r_p} =$	35
$W_{r_a} =$	25
$W_a =$	2
$W_\omega =$	170
$W_e = W_i = W_{\Omega=}$	0

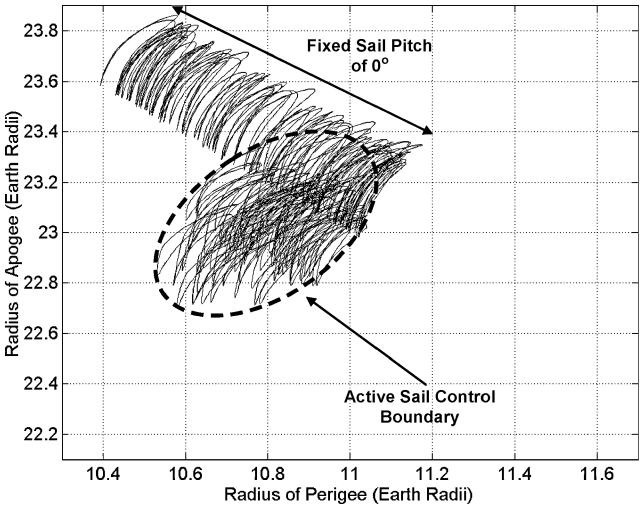

Fig. 9 Displacement of perigee and apogee from nominal values, fixed and active sail control.

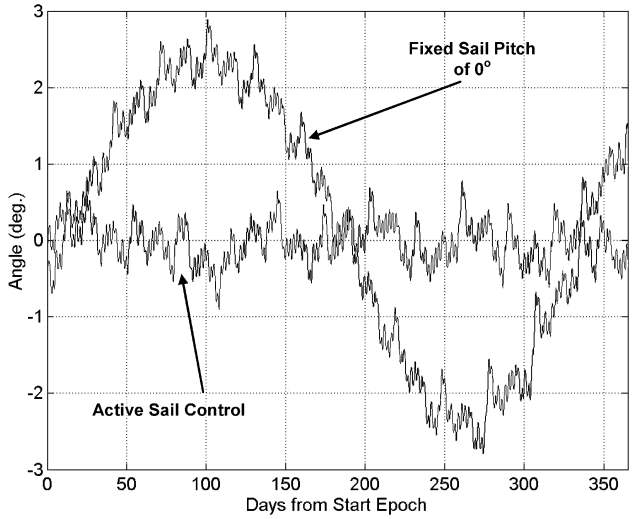

Fig. 10 Variation in angle between Earth–sun line and orbit major axis, fixed and active sail control.

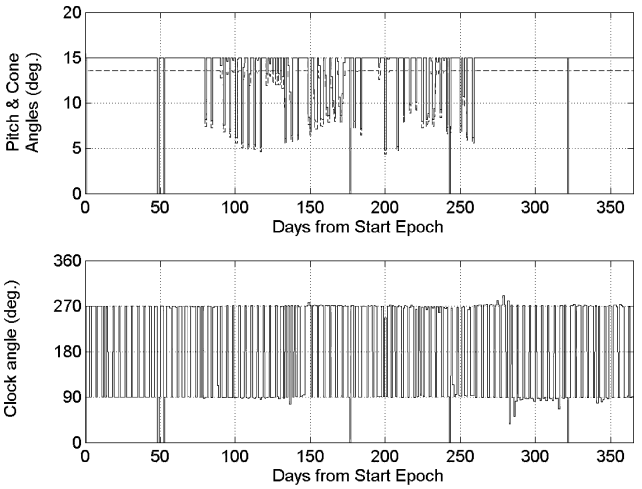

Fig. 11 Active sail control angles selected by using A^{n}D blending.

science mission, and as such the primary science requirement is for accurate control of apogee and the argument of perigee; thus, no such adjustment was adopted.

Figure 10 shows the variation in the angle between the Earth–sun line and the orbit major axis for a fixed and active sail. We note that the orbit major axis and Earth–sun line vary by as much as 3 deg for a fixed sail pitch, while the A^{n}D blending method reduces this variation to less than 1 deg. Finally, we see in Fig. 11 the sail control angles generated by the A^{n}D blending method for the GeoSail scenario with active sail control. We define sail pitch angle as the angle from the sail-sun line to the sail normal, whereas the sail cone angle is the angle from the sail-sun line to the sail thrust vector. The sail cone angle equals the sail pitch angle for an ideal sail only and is less than the pitch angle for a nonideal sail. We note that typically the sail pitch angle is 15 deg with the clock angle flipping the sail thrust vector either left or right of the orbit major axis. As such, the maximum required sail slew angle between discrete sail pitch settings is 30 deg; however, we also note that at other times the sail does not move for as much as three to five days. We can thus define the technology requirement for sail slew capabilities in an active sail mission scenario as 30 deg in 1.25–2.5 h, 5–10% of the duration of each discrete sail setting. Thus, the time for each slew maneuver is significantly less than the duration of each discrete set of control angles. GeoSail is a demonstration class mission; thus, as part of an extended mission active sail control using A^{n}D blending could be demonstrated over and above the basic solar sail demonstration capabilities of the GeoSail mission.

Conclusions

A new method of assessing the relative importance of orbit elements during solar-sail transfer and stationkeeping maneuvers has been introduced, allowing rapid generation of trajectories by blending locally optimal control laws. The accessibility and deficit (A^{n}D) blending method considers both an orbital element's variance from its target value and how well that orbital element will use the sail prior to calculating a score for the element. A^{n}D blending directs the blended locally optimal force vector such that it avoids prolonged periods of high sail pitch settings, which are an inefficient use of the sail, thus increasing sail efficiency.

The A^{n}D blending method has been demonstrated for generation of a complex orbit transfer at Mercury, where the primary cost function of the transfer was thermal rather than time. The transfer trajectory rotates argument of pericenter by 180 deg, while continually retargeting toward a new ascending node final value, which is initially rotated 180 deg from the trajectory's starting ascending node value. The trajectory is verified shadow free, and all orbit elements converge well with the target values. The use of A^{n}D blending allows the generation of such a transfer trajectory in a much more rapid fashion than would be possible with conventional optimization techniques.

Furthermore, A^{n}D blending has been demonstrated to act as an excellent solar-sail stationkeeping algorithm, capable of adjusting to significant variations in orbit perturbation magnitude. The control method demonstrated is capable of providing the sail control angles in real time, based solely on the current spacecraft state vectors. Thus, these two factors combined make A^{n}D blending suitable as a potential autonomous onboard sail control system.

References

[1]McInnes, C. R., *Solar Sailing: Technology, Dynamics and Mission Applications*, Springer-Verlag, London, 1999.

[2]Hughes, G., Macdonald, M., McInnes, C. R., and Atzei, A., "Terrestrial Planet Sample Return Using Solar Sail Propulsion," *Proceedings of Fifth IAA International Conference on Low-Cost Planetary Missions*, ESA SP-542, Noordwijk, The Netherlands, 2003, pp. 377–384.

[3]Sands, N., "Escape from Planetary Gravitational Fields by Using Solar Sails," *ARS Journal*, Vol. 31, April 1961, pp. 527–531.

[4]Fimple, W. R., "Generalized Three-Dimensional Trajectory Analysis of Planetary Escape by Solar Sail," *ARS Journal*, Vol. 32, June 1962, pp. 883–887.

[5]Coverstone-Carroll, V., and Prussing, J. E., "A Technique for Earth Escape Using a Solar Sail," *Advances in the Astronautical Sciences*, Vol. 103, Pt. 1, 1999, pp. 507–523.

[6]Coverstone, V. L., and Prussing, J. E., "Technique for Earth Escape from Geosynchronous Transfer Orbit Using a Solar Sail," *Journal of Guidance, Control, and Dynamics*, Vol. 26, No. 4, 2003, pp. 628–634.

[7]Fekete, T. A., Sackett, L. L., and von Flotow, A. H., "Trajectory Design for Solar Sailing from Low-Earth Orbit to the Moon," *Advances in the Astronautical Sciences*, Vol. 79, Pt. 3, 1992, pp. 1083–1094.

[8]Eguchi, S., Ishii, N., and Matsuo, H., "Guidance Strategies for Solar Sail to the Moon," *Advances in the Astronautical Sciences*, Vol. 85, Pt. 2, 1993, pp. 1419–1433.

[9]Morgan, T. O., "The Inclination Change for Solar Sails and Low Earth Orbit," *Advances in the Astronautical Sciences*, AAS/AIAA Astrodynamics Conf., AAS Paper 79-104, 1979.

[10]Sackett, L. L., "Optimal Solar Sail Planetocentric Trajectories," R-1113, The Charles Stark Draper Lab., Inc., JPL–NASA Contract NAS 7-100 Final Rept., Cambridge, MA, Sept. 1977.

[11]Sackett, L. L., and Edelbaum, T. N., "Optimal Solar Sail Spiral to Escape," AAS/AIAA Astrodynamics Conf., AAS Paper A78 31-901, 1978.

[12]Leipold, M., "Solar Sail Mission Design," Ph.D. Dissertation, Technische Univ. München, DLR-Forschungsbericht 2000-22, 2000.

[13]Macdonald, M., and McInnes, C. R., "Realistic Earth Escape Strategies for Solar Sailing," *Journal of Guidance, Control, and Dynamics*, Vol. 28, No. 2, 2005, pp. 315–323.

[14]Macdonald, M., and McInnes, C. R., "Analytic Control Laws for Near-Optimal Geocentric Solar Sail Transfers," *Advances in the Astronautical Sciences*, Vol. 109, No. 3, 2001, pp. 2393–2413.

[15]Kluever, C. A., "Simple Guidance Scheme for Low-Thrust Orbit Transfers," *Journal of Guidance, Control, and Dynamics*, Vol. 21, No. 6, 1998, pp. 1015–1017.

[16]Schoenmaekers, J., Pulido, J., and Jehn, R., "SMART-1 Mission Analysis: Moon Option," ESOC Rept. S1-ESC-RP-5001, No. 1, ESA Publications, Darmstadt, Germany, Sept. 1998.

[17]Petropoulos, A. E., "Simple Control Laws for Low-Thrust Orbit Transfers," *Advances in the Astronautical Sciences*, Vol. 116, Pt. 3, 2003, pp. 2031–2049.

[18]Green, A. J., "Optimal Escape Trajectories From a High Earth Orbit by Use of Solar Radiation Pressure," M.S. Thesis, T-652, Massachusetts Inst. of Technology, Cambridge, MA, 1977.

[19]Pagel, G., "Extremale Steuerstrategien für Sonnensegler am Beispiel von Bahntransferproblemen zum Erdmond," Ph.D. Dissertation, Technischen Univ., Berlin, May 2002 (in German).

[20]Sackett, L. L., "Optimal Solar Sail Planetocentric Trajectories," R-1113, The Charles Stark Draper Lab., Inc., JPL–NASA Contract NAS 7-100 Final Rept., Cambridge, MA, Sept. 1977.

[21]Sackett, L. L., and Edelbaum, T. N., "Optimal Solar Sail Spiral to Escape," *Advances in the Astronautical Sciences*, Paper A78 31-901, 1978.

[22]Leipold, M., Borg, E., Lingner, S., Pabsch, A., Sachs, R., and Seboldt, W., "Mercury Orbiter with a Solar Sail Spacecraft," *Acta Astronautica*, Vol. 35, Suppl., 1995, pp. 635–644.

[23]Leipold, M., Borg, E., Lingner, S., Pabsch, A., Sachs, R., and Seboldt, W., "Mercury Sun-Synchronous Polar Orbiter with a Solar Sail," *Acta Astronautica*, Vol. 39, No. 1–4, 1996, pp. 143–151.

[24]Leipold, M. E., and Wagner, O., "Mercury Sun-Synchronous Polar Orbits Using Solar Sail Propulsion," *Journal of Guidance, Control, and Dynamics*, Vol. 19, No. 6, 1996, pp. 1337–1341.

[25]Dormand, J. R., and Price, P. J., "A Family of Embedded Runge–Kutta Formulae," *Journal of Computing and Applied Mathematics*, Vol. 6, 1980, pp. 19–26.

[26]Burt, E. G. C., "On Space Manoeuvres with Continuous Thrust," *Planet Space Science*, Vol. 15, 1967, pp. 103–122.

[27]Roy, A. E., *Orbital Motion*, Inst. of Physics Publishing, London, 1998.

[28]McInnes, C., Macdonald, M., Angelopous, V., and Alexander, V., "GEOSAIL: Exploring the Geomagnetic Tail Using a Small Solar Sail," *Journal of Spacecraft and Rockets*, Vol. 38, No. 4, 2001, pp. 622–629.